

Model Order Estimation for A Sum of Complex Exponentials

Raymundo Albert, Cecilia G. Galarza

Abstract—In this paper, we present a new method for estimating the number of terms in a sum of exponentially damped sinusoids embedded in noise. In particular, we propose to combine the shift-invariance property of the Hankel matrix associated with the signal with a constraint over its singular values to penalize small order estimations. With this new methodology, the algebraic and statistical structures of the Hankel matrix are considered. The new order estimation technique shows significant improvements over subspace-based methods. In particular, when a good separation between the noise and the signal subspaces is not possible, the new methodology outperforms known techniques. We evaluate the performance of our method using numerical experiments and comparing its performance with previous results found in the literature.

Index Terms—Spectral estimation, subspace-based methods, optimal threshold, model order selection.

I. INTRODUCTION

A ubiquitous problem in signal processing is to recover useful information from a signal modeled as a sum of complex exponentials. This problem is significant in applications such as radar [1], spectroscopy [2], and music signals [3], to mention just a few. The signal to be detected usually contains unknown parameters such as amplitude, phase, frequency, etc. Subspace-based techniques [4] have shown good performance for estimating the model parameters by solving spectral estimation problems. Moreover, recent studies based in convex optimization have reported new procedures that exhibit good performance under different setups [5], [6]. Nevertheless, a sensible step in any parametric spectral estimation method is to accurately estimate the model order.

The seminal works applied information-theoretic criteria to estimate the model order [7]. The Akaike Information Criterion, the Minimum Description Length, as well as a more recent approach developed in [8], guarantee good performance in the asymptotic case. However, for short data records, these methods are no longer optimal and they loose performance when the Signal-to-Noise Ratio (SNR) is low.

An alternative strategy uses Kronecker's theorem that states a one-to-one correspondence between a linear combination of r complex exponentials and a Hankel matrix with rank r . Unfortunately, this result is difficult to apply in real-life implementations, because noise contaminates the observed signal. In consequence, the Hankel matrix has full rank. Using a Singular Value Decomposition (SVD) of the Hankel matrix, it is possible to decompose its columns space in a dominant subspace related to the signal and a secondary subspace known as the noise-subspace. The dimension of the signal subspace is established by the number of prominent singular values. In

the low SNR regime, there is no clear cut between singular values. Then, determining which ones are the relevant singular values becomes a difficult task. Recently, the authors in [9], [10] have addressed this problem. In particular, they have studied a non-random matrix perturbed by a noise matrix with zero mean independent and identically distributed (i.i.d) entries. For this case, they proposed a universal threshold to separate the dominant singular values of the observed matrix. In their presentation, they analyzed the statistical behavior of the singular values of Gaussian matrices. Another method along these lines includes a detection strategy that takes into account the statistical properties of eigenvalues of Gaussian matrices [11]. These approaches are attractive, and they show good performance when the Signal-to-Noise Ratio (SNR) is low. However, they have poor performance when applied to Hankel matrix because they discard the statistics induced by the Hankel structure.

In [12] another hard threshold for singular values was proposed for random real matrices with subgaussians entries and Toeplitz structure. When dealing with random Hankel matrix with Gaussian entries, a similar bound can be found using concentration inequalities [13]. More general random Hankel matrices were studied in [14]. The authors found the hard threshold as an upper bound on the spectral norm of the random Hankel matrix. Nonetheless, this is a conservative bound that underestimates the matrix rank.

The methods mentioned above select the model order by analyzing the spectral properties of the additive noise. Alternatively, other methods exploit the structure of the data. In the case of a Hankel matrix constructed from a sum of complex exponentials, the rotational invariance is a well-known principle employed in spectrum estimation techniques [15]. The authors in [16] followed this path to propose the order selection technique known as ESTER. Although they showed good performance when combined with the algorithm ESPRIT for spectrum estimation, ESTER is based on noiseless assumptions. An alternative technique was proposed in [17] and it was called SAMOS. While SAMOS is more robust than ESTER, both techniques work well in the high SNR regime, but they fail when the signal is not strong enough.

In this work, we analyze some of the pitfalls of these schemes and propose a new alternative that is resilient to high noise power, while keeping it accurate when the signal gets stronger. In particular, we propose to combine the shift-invariance property of the Hankel matrix associated with the sum of exponentials with a constraint on the singular values associated with noise in a single optimization problem. In this way, we are taking into account not only the algebraic structure

of the signal but also its statistical properties.

The rest of the paper is organized as follows: in section II we introduce the signal model and present the rotational invariance property. Section III reviews some techniques for model order estimation and points out their drawbacks in the context of the model introduced before. In section IV we find bounds for the spectral norm of a random Hankel matrix. Section V introduces our proposal. In section VI we perform Montecarlo simulation to compare the performance of our proposed method with other popular. Finally section VII concludes the paper with final remarks.

A. Notation

Throughout the paper we use standard notation: lowercase (v) for scalars, boldface lowercase (\mathbf{v}) for vectors, uppercase boldface \mathbf{A} for matrices. Given a matrix \mathbf{A} , we denote its transpose, Hermitian, and Moore-Penrose pseudo-inverse as \mathbf{A}^T , \mathbf{A}^H , \mathbf{A}^\dagger respectively. $\|\mathbf{A}\|_2$ is reserved for the induced 2-norm. The notation \mathbf{I}_m is used for the $m \times m$ identity matrix. We use calligraphic letters (\mathcal{X}) for subspaces.

II. MODEL DESCRIPTION

Consider the following model

$$y_k = x_k + w_k, \quad k = 0, 1, \dots, \quad (1)$$

where x_k is given by

$$x_k = \sum_{i=1}^r c_i z_i^k \quad k = 0, 1, \dots, \quad (2)$$

w_k is a circularly symmetric complex Gaussian process, $w_k \sim \mathcal{CN}(0, \eta^2)$, $z_i \in \mathbb{C}$ is a complex resonant frequency, and $c_i \in \mathbb{C}$ the amplitude associated with it. The goal is to estimate r using the samples y_k , $k = 0, 1, \dots, N-1$. An appropriate model order estimation is key for an accurate estimation of the resonances z_i .

Given $m, n > 0$, define the $m \times n$ -Hankel matrix, $\mathcal{H}_{\mathbf{x}}$ obtained from x_0, \dots, x_{m+n-2}

$$\mathcal{H}_{\mathbf{x}} = \begin{bmatrix} x_0 & x_1 & \cdots & x_{n-1} \\ x_1 & x_2 & \cdots & x_{n-2} \\ \vdots & & & \vdots \\ x_{m-1} & x_{m-2} & \cdots & x_{m+n-2} \end{bmatrix}. \quad (3)$$

Since x_k satisfies (2), we know that the rank of $\mathcal{H}_{\mathbf{x}}$ is r . Now, consider the Singular Value Decomposition (SVD)

$$\mathcal{H}_{\mathbf{x}} = \mathbf{U}\mathbf{\Lambda}\mathbf{V}, \quad (4)$$

where $\mathbf{\Lambda}$ is a diagonal matrix that contains the singular values arranged in decreasing order. Then, $\mathbf{U}(r)$, which contains the first r singular vectors of $\mathcal{H}_{\mathbf{x}}$, spans the signal space. Let us define the following matrices

$$\begin{aligned} \mathbf{U}_f(r) &= [\mathbf{0}_{(m-1) \times 1} \quad \mathbf{I}_{m-1}] \mathbf{U}(r), \\ \mathbf{U}_l(r) &= [\mathbf{I}_{m-1} \quad \mathbf{0}_{(m-1) \times 1}] \mathbf{U}(r). \end{aligned} \quad (5)$$

Efficient spectral estimation techniques such as ESPRIT [18], exploit the rotational invariance property of $\mathcal{H}_{\mathbf{x}}$,

$$\mathbf{U}_f(r) = \mathbf{U}_l(r)\mathbf{\Phi}. \quad (6)$$

Here $\mathbf{\Phi} \in \mathbb{C}^{r \times r}$ is a non-singular matrix. According to (6), $\mathbf{U}_f(r)$ and $\mathbf{U}_l(r)$ span the same subspace. Then, if $\mathcal{H}_{\mathbf{x}}$ were available, a plausible order estimation approach would be to find the integer r that satisfies (6). Unfortunately, the signal x_k is observed only through a noisy version y_k as in (1). Let $\mathcal{H}_{\mathbf{y}}$ be the $m \times n$ -Hankel matrix built from y_0, \dots, y_{m+n-2} .

$$\mathcal{H}_{\mathbf{y}} = \mathcal{H}_{\mathbf{x}} + \mathcal{H}_{\mathbf{w}}, \quad (7)$$

where $\mathcal{H}_{\mathbf{w}}$ is a perturbation matrix that has a Hankel structure. For future reference, we introduce the following SVD

$$\mathcal{H}_{\mathbf{y}} = \mathbf{Q}\mathbf{\Sigma}\mathbf{P}. \quad (8)$$

In the sequel, we consider model order selection schemes that use $\mathcal{H}_{\mathbf{y}}$ to estimate an appropriate order.

III. MODEL ORDER SELECTION RULES

Model order selection techniques may estimate the dimension of the signal space using statistical information about the noisy observations [7]. Also, when the signal model satisfies (2), we can benefit from its particular algebraic structure, as in (6) [17], [19]. In this section, we review three different techniques for model order selection. The first two are only suitable for models that satisfy the rotational invariance property. On the other hand, the third one only considers the nuisance of the random perturbation onto the signal.

A. Algebraic Structure of the Signal

Suppose that $\mathcal{H}_{\mathbf{x}}$ is available, i.e., we are in the noiseless case. Define the matrix $\mathbf{U}(s) \in \mathbb{C}^{m \times s}$ that contains the first s columns of \mathbf{U} , and $\mathbf{U}_f(s)$ and $\mathbf{U}_l(s)$ following (5). When $s = r$, $\mathbf{U}_f(s)$ and $\mathbf{U}_l(s)$ span the same subspace according to (6). The closeness between the column spaces of $\mathbf{U}_f(s)$ and $\mathbf{U}_l(s)$ provides a key to estimate r . We use the principal angles as a measure of proximity between subspaces.

Definition 1. Let $\mathcal{X}, \mathcal{Y} \subseteq \mathbb{C}^n$ be complex subspaces with $\dim(\mathcal{X}) = \dim(\mathcal{Y}) = s$. The principal angles between \mathcal{X} and \mathcal{Y} are

$$\Theta(\mathcal{X}, \mathcal{Y}) = [\theta_1, \dots, \theta_s], \quad \theta_k \in [0, \pi/2], \quad k = 1, \dots, s$$

which are recursively defined by

$$\begin{aligned} \cos \theta_k &= \frac{|\langle \mathbf{x}_k, \mathbf{y}_k \rangle|}{\|\mathbf{x}_k\|_2 \|\mathbf{y}_k\|_2} \\ &= \max_{\substack{\mathbf{x} \in \mathcal{X} \\ \mathbf{y} \in \mathcal{Y}}} \left\{ \frac{|\langle \mathbf{x}, \mathbf{y} \rangle|}{\|\mathbf{x}\|_2 \|\mathbf{y}\|_2} : \mathbf{x}^H \mathbf{x}_i = 0, \mathbf{y}^H \mathbf{y}_i = 0, \right. \\ &\quad \left. \forall i \in \{1, \dots, k-1\} \right\}. \end{aligned} \quad (9)$$

The vectors $\{\mathbf{x}_1, \dots, \mathbf{x}_s\}$ and $\{\mathbf{y}_1, \dots, \mathbf{y}_s\}$ are called the principal vectors.

Lemma 1. $\mathcal{X} = \mathcal{Y}$, if and only $\Theta(\mathcal{X}, \mathcal{Y}) = 0$

Proof. By construction, the principal vectors $\{\mathbf{x}_1, \dots, \mathbf{x}_s\}$ are linearly independent vectors that span the subspace \mathcal{X} because $\dim(\mathcal{X}) = s$. Similarly, the principal vectors $\{\mathbf{y}_1, \dots, \mathbf{y}_s\}$ span \mathcal{Y} . If $\cos \theta_k = 1$, we have that \mathbf{x}_k and \mathbf{y}_k are aligned. Therefore, if all the principal angles are zero, the sets $\{\mathbf{x}_1, \dots, \mathbf{x}_s\}$ and $\{\mathbf{y}_1, \dots, \mathbf{y}_s\}$ generate the same subspace.

On the other hand, when $\mathcal{X} = \mathcal{Y}$, it is clear that

$$\max_{\substack{\mathbf{x} \in \mathcal{X} \\ \mathbf{y} \in \mathcal{Y}}} \frac{|\langle \mathbf{x}, \mathbf{y} \rangle|}{\|\mathbf{x}\|_2 \|\mathbf{y}\|_2} = 1$$

and therefore, $\cos \theta_k = 1$ for all k . \square

Definition 2. The gap distance between \mathcal{X} and \mathcal{Y} is given by

$$\rho(\mathcal{X}, \mathcal{Y}) = \max \left\{ \max_{\substack{\mathbf{x} \in \mathcal{X} \\ \|\mathbf{x}\|_2=1}} \text{dist}(\mathbf{x}, \mathcal{Y}), \max_{\substack{\mathbf{y} \in \mathcal{Y} \\ \|\mathbf{y}\|_2=1}} \text{dist}(\mathbf{y}, \mathcal{X}) \right\}, \quad (10)$$

Proposition 1. Let \mathcal{X} and \mathcal{Y} be two subspaces, and denote $\mathcal{P}_{\mathcal{X}}$ and $\mathcal{P}_{\mathcal{Y}}$ the orthogonal projections onto \mathcal{X} and \mathcal{Y} respectively. Then

- i) $\rho(\mathcal{X}, \mathcal{Y}) = \|\mathcal{P}_{\mathcal{X}} - \mathcal{P}_{\mathcal{Y}}\|_2$;
- ii) $\rho(\mathcal{X}, \mathcal{Y}) = \sin \theta_1$, with θ_1 the maximum principal angle between \mathcal{X} and \mathcal{Y} .

Proof. The proof of this proposition is in [20, Th.4.5]. \square

Let $\mathcal{P}_f(s)$ and $\mathcal{P}_l(s)$ be the projection matrices onto the column spaces of $\mathbf{U}_f(s)$ and $\mathbf{U}_l(s)$ respectively. Define $\theta_1(s) \geq \dots \geq \theta_s(s)$ as the principal angles between the s -dimension column-spaces of $\mathbf{U}_f(s)$ and $\mathbf{U}_l(s)$. According to Proposition 1, the gap distance between $\mathbf{U}_f(s)$ and $\mathbf{U}_l(s)$ is

$$\rho(s) = \|\mathcal{P}_f(s) - \mathcal{P}_l(s)\|_2 = \sin \theta_1(s) \quad (11)$$

Theorem 1. Consider the function

$$\mathbf{E}(s) = \mathbf{U}_f(s) - \mathbf{U}_l(s)\mathbf{U}_l(s)^\dagger \mathbf{U}_f(s), \quad (12)$$

Then $\|\mathbf{E}(s)\|_2 \leq \sin \theta_1(s)$.

Proof. Consider the polar decomposition of $\mathbf{U}_f(s)$ and $\mathbf{U}_l(s)$

$$\begin{aligned} \mathbf{U}_f(s) &= \hat{\mathbf{U}}_f(s)(\mathbf{I}_s - \mathbf{u}_f^H \mathbf{u}_f)^{\frac{1}{2}} \\ \mathbf{U}_l(s) &= \hat{\mathbf{U}}_l(s)(\mathbf{I}_s - \mathbf{u}_l^H \mathbf{u}_l)^{\frac{1}{2}} \end{aligned} \quad (13)$$

where $\mathbf{u}_f \in \mathbb{C}^{1 \times s}$ ($\mathbf{u}_l \in \mathbb{C}^{1 \times s}$) is the first (last) row of $\mathbf{U}(s)$, and $\hat{\mathbf{U}}_f(s)$ and $\hat{\mathbf{U}}_l(s)$ are $(m-1) \times s$ -complex matrices, both with orthonormal columns. The orthogonal projections onto the column spaces of $\mathbf{U}_f(s)$ and $\mathbf{U}_l(s)$ are:

$$\begin{aligned} \mathcal{P}_f(s) &= \mathbf{U}_f(s)\mathbf{U}_f(s)^\dagger = \hat{\mathbf{U}}_f(s)\hat{\mathbf{U}}_f^H(s) \\ \mathcal{P}_l(s) &= \mathbf{U}_l(s)\mathbf{U}_l(s)^\dagger = \hat{\mathbf{U}}_l(s)\hat{\mathbf{U}}_l^H(s), \end{aligned} \quad (14)$$

where $\mathbf{U}_l(s)^\dagger$ is the Moore-Penrose pseudo-inverse. Now, let

$$\hat{\mathbf{E}}(s) = \hat{\mathbf{U}}_f(s) - \hat{\mathbf{U}}_l(s)\hat{\mathbf{U}}_l^H(s)\hat{\mathbf{U}}_f(s). \quad (15)$$

Since $\hat{\mathbf{U}}_f$ and $\hat{\mathbf{U}}_l$ have orthonormal columns

$$\begin{aligned} \|\hat{\mathbf{E}}(s)\|_2 &= \|\hat{\mathbf{U}}_f(s) - \hat{\mathbf{U}}_l(s)\hat{\mathbf{U}}_l^H(s)\hat{\mathbf{U}}_f(s)\|_2 \\ &= \left\| \left(\hat{\mathbf{U}}_f(s)\hat{\mathbf{U}}_f^H(s) - \hat{\mathbf{U}}_l(s)\hat{\mathbf{U}}_l^H(s) \right) \hat{\mathbf{U}}_f(s) \right\|_2 \\ &= \|\mathcal{P}_f(s) - \mathcal{P}_l(s)\|_2 = \rho(s) \end{aligned}$$

where we have used Proposition 1 in the last equality. Now,

$$\begin{aligned} \|\mathbf{E}(s)\|_2 &= \|\mathbf{U}_f(s) - \mathbf{U}_l(s)\mathbf{U}_l(s)^\dagger \mathbf{U}_f(s)\|_2 \\ &= \left\| \left(\mathbf{U}_f(s)\mathbf{U}_f(s)^\dagger - \mathbf{U}_l(s)\mathbf{U}_l(s)^\dagger \right) \mathbf{U}_f(s) \right\|_2 \\ &\leq \|\mathcal{P}_f(s) - \mathcal{P}_l(s)\|_2 \|\mathbf{U}_f(s)\|_2 \\ &= \rho(s) \|\mathbf{U}_f(s)\|_2. \end{aligned} \quad (16)$$

Since $\mathbf{U}_f(s)$ is a submatrix of the unitary matrix \mathbf{U} , its singular values will be at most 1. Then $\|\mathbf{U}_f(s)\|_2 \leq 1$ and the result follows. \square

Theorem 2. Define the augmented matrix

$$\mathbf{E}_{aug}(s) = [\mathbf{U}_f(s) \quad \mathbf{U}_l(s)]. \quad (17)$$

Let $\gamma_1 \geq \dots \geq \gamma_{2s}$ be its singular values. Then,

$$\frac{1}{s} \sum_{i=s+1}^{2s} \gamma_i \leq \sqrt{2} \left[1 + \frac{1}{s} \sum_{i=1}^s \sin \frac{\theta_i(s)}{2} \right] \quad (18)$$

Proof. Recalling that $\mathbf{U}_f(s)$ is a full rank matrix, we have that $\mathbf{U}_f(s)$ and $\hat{\mathbf{U}}_f(s)$ span the same column space, and likewise $\mathbf{U}_l(s)$ and $\hat{\mathbf{U}}_l(s)$. Then, the principal angles between $\mathbf{U}_f(s)$ and $\mathbf{U}_l(s)$ are the same as the angles between $\hat{\mathbf{U}}_f(s)$ and $\hat{\mathbf{U}}_l(s)$. Define

$$\hat{\mathbf{E}}_{aug}(s) = [\hat{\mathbf{U}}_f(s) \quad \hat{\mathbf{U}}_l(s)]. \quad (19)$$

Notice that the singular values of $\hat{\mathbf{E}}_{aug}(s)$ are obtained from the matrix $\mathbf{I}_{2s} + \mathbf{M}$, where

$$\mathbf{M} = \begin{bmatrix} \mathbf{0} & \hat{\mathbf{U}}_f(s)^H \hat{\mathbf{U}}_l(s) \\ \hat{\mathbf{U}}_l(s)^H \hat{\mathbf{U}}_f(s) & \mathbf{0} \end{bmatrix}.$$

According to [20, Th. I.5.2], the singular values of $\hat{\mathbf{U}}_f(s)^H \hat{\mathbf{U}}_l(s)$ arranged in non-increasing order are $\cos \theta_1(s), \dots, \cos \theta_s(s)$. Then, from [21, Th. 7.3.3], the last s singular values of $\hat{\mathbf{E}}_{aug}$ arranged in non-increasing order are

$$\sqrt{1 - \cos \theta_{2s-i+1}(s)} = \sqrt{2} \sin \frac{\theta_{2s-i+1}(s)}{2} \quad i = s+1, \dots, 2s.$$

Let $\mathbf{A} = \mathbf{U}_f(s) - \hat{\mathbf{U}}_f(s)$, and $\mathbf{B} = \mathbf{U}_l(s) - \hat{\mathbf{U}}_l(s)$. Therefore, $\mathbf{E}_{aug}(s) - \hat{\mathbf{E}}_{aug}(s) = [\mathbf{A} \quad \mathbf{B}]$. It was proven in [22] that $\hat{\mathbf{U}}_f(s)$ is the nearest matrix to $\mathbf{U}_f(s)$ with orthonormal columns, and so is $\hat{\mathbf{U}}_l(s)$ with $\mathbf{U}_l(s)$. Moreover,

$$\|\mathbf{A}\|_2 = \max_i |\zeta_i - 1|,$$

where ζ_i is the i -th largest singular value of $\mathbf{U}_f(s)$. Notice that $\zeta_i \leq 1$ because $\mathbf{U}_f(s)$ is a submatrix of the unitary matrix \mathbf{U} . Therefore, $\|\mathbf{A}\|_2 \leq 1$, and similarly, $\|\mathbf{B}\|_2 \leq 1$. According to Weyl Theorem [20, Th. 4.11], the last s singular values of $\mathbf{E}_{aug}(s)$ and $\hat{\mathbf{E}}_{aug}(s)$ are separated at most by $\|\mathbf{A} \quad \mathbf{B}\|_2$, i.e., for $i = s+1, \dots, 2s$,

$$\begin{aligned} \left| \gamma_i - \sqrt{2} \sin \frac{\theta_{2s+1-i}(s)}{2} \right| &\leq \|\mathbf{A} \quad \mathbf{B}\|_2 \\ &\leq \sqrt{\|\mathbf{A}\|_2^2 + \|\mathbf{B}\|_2^2} \leq \sqrt{2}. \end{aligned} \quad (20)$$

Using the triangle inequality we get

$$\begin{aligned} & \frac{1}{s} \sum_{i=s+1}^{2s} \gamma_i - \frac{1}{s} \sum_{i=s+1}^{2s} \sqrt{2} \sin \frac{\theta_{2s+1-i}(s)}{2} \leq \\ & \leq \frac{1}{s} \sum_{i=s+1}^{2s} \left| \gamma_i - \sqrt{2} \sin \frac{\theta_{2s+1-i}(s)}{2} \right| \leq \sqrt{2}. \end{aligned}$$

Then,

$$\frac{1}{s} \sum_{i=s+1}^{2s} \gamma_i \leq \sqrt{2} + \frac{1}{s} \sum_{i=1}^s \sqrt{2} \sin \frac{\theta_i(s)}{2},$$

where we have rearranged the terms in the last summation. \square

We have shown experimentally that both Theorems 1 and 2 provide tight upper bounds. For that, we have simulated (2) using different values for r . For each signal, the frequencies $z_i = e^{2\pi j f_i}$ were selected by taking r frequencies uniformly spread in the interval $(0, 1]$. The complex amplitudes c_i were independent samples of the uniform distribution in $[1, 1.5]$. Fig. 1 shows the results as s varies. To assess the bound in Th. 1, Fig.1(a) shows $\|\mathbf{E}(s)\|_2 - \rho(s)$. Th. 2 is analyzed in Fig. 1(b) that displays $1/s |\sum_{i=1}^s (\gamma_{s+i} - \sqrt{2} \sin(\theta_i(s)/2))|$. Both figures show that the bounds are tight for all s . Moreover, they are both minimized when $s = r$.

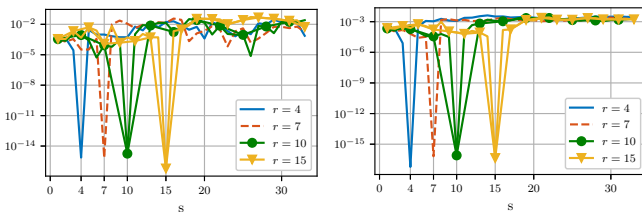
When $s = r$, the column spaces of $\mathbf{U}_f(s)$ and $\mathbf{U}_l(s)$ are aligned. Then, all the angles $\theta_i(s)$, $i = 1, \dots, s$, are equal to zero. Therefore, $\rho(s) = 0$ and we obtain the right order by minimizing $\|\mathbf{E}(s)\|_2$. Also in this case, $\text{rank}(\mathbf{E}_{aug}(s)) = r$, $\gamma_{s+1} = \dots = \gamma_{2s} = 0$, and minimizing (18) is also a good alternative. However, both observations rely on the knowledge of matrix \mathbf{U} , which is only possible in the noiseless case.

Since \mathcal{H}_x is only observed thru \mathcal{H}_y , \mathbf{U} is not directly known, and we have to work with \mathbf{Q} and its submatrices instead. Using these matrices, the order estimation rule known as ESTimation Error Rule (ESTER) was proposed in [16]. The rule minimizes the function

$$J_{ESTER}(s) = \|\mathbf{Q}_f(s) - \mathbf{Q}_l(s)\mathbf{Q}_l(s)^\dagger\mathbf{Q}_f(s)\|_2. \quad (21)$$

An alternative approach, the subspace-based automatic model order selection (SAMOS), was proposed in [17]. In this case, the rule selects the order that minimizes the sum of ζ_i , $i = s+1, \dots, 2s$, which are the last singular values of $[\mathbf{Q}_f(s) \ \mathbf{Q}_l(s)]$

$$J_{SAMOS}(s) = \frac{1}{s} \sum_{i=s+1}^{2s} \zeta_i. \quad (22)$$



(a) $\|\mathbf{E}(s)\|_2 - \rho(s)$ (b) $|\sum_i (\gamma_{s+i} - \sqrt{2} \sin(\theta_i/2))|$

Fig. 1: Evaluation of the bounds given in Th. 1 and 2.

Let $\vartheta_i(s), i = 1, \dots, s$ be the principal angles between $\mathbf{Q}_l(s)$ and $\mathbf{Q}_f(s)$ ordered in non-increasing order. Th. 1 and 2 state upper bounds for the cost used in the ESTER and SAMOS methods. Notably,

$$J_{ESTER}(s) \leq \sin \vartheta_1(s). \quad (23)$$

$$J_{SAMOS}(s) \leq \sqrt{2} \left[1 + \frac{1}{s} \sum_{i=1}^s \sin \frac{\vartheta_i(s)}{2} \right]. \quad (24)$$

It was shown in [17], [19] that these methods outperform information-theoretic criteria such as AIC or MDL. However, these techniques do not have good performance under high noise level. Notice that when s is close to r the angles $\vartheta_i(s), i = 1, \dots, s$ are small, and $\sin(\vartheta_i(s))$ is very sensitive to small deviations. As a consequence, both techniques have a poor performance when the noise level is high as it was observed experimentally. Although in SAMOS the average shown in (24) may reduce the effect of noise, this is not completely effective when we are dealing with low signal to noise ratios. In section VI we show some numerical experiments that support these claims.

B. Statistical Structure of the Noise

A different approach for model order estimation is to infer $\text{rank}(\mathcal{H}_x)$ by counting the relevant singular values of \mathcal{H}_y . When given a hard threshold τ , the model order is estimated as

$$\hat{r}_{thr} = |\{\sigma_i : \sigma_i > \tau\}|. \quad (25)$$

Here $|\cdot|$ is the size of the set. The choice of τ is a delicate matter. A large value for τ could result in selecting a rank lower than desired. On the other hand, a small τ leads to overestimating the model order. This problem was studied in [9], where the authors considered a perturbation matrix with independent identically distributed (i.i.d.) entries. Under an appropriate asymptotic framework, the authors obtain that the optimal value for τ is

$$\tau = \kappa \sqrt{m\eta} \quad (26)$$

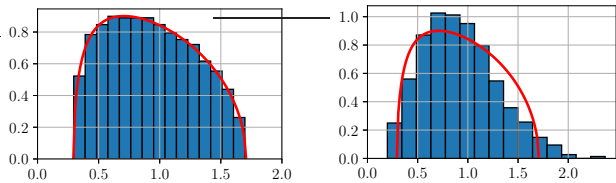
where η is the white noise level and κ is a constant that depends on the matrix dimensions

$$\kappa = \sqrt{2(c+1) \frac{8c}{c+1 + \sqrt{c^2 + 14c + 1}}}.$$

The result follows from the limiting distribution of the singular values of a matrix with i.i.d. entries. Let \mathbf{W} be a $m \times n$ matrix ($m \geq n$) with i.i.d. entries. Denote $c = \frac{n}{m}$. Then the empirical distribution of the singular values of \mathbf{W}/\sqrt{m} follows the Marchenko-Pastur density

$$f_{MP}(x) = \frac{\sqrt{4c - (x^2 - 1 - c)^2}}{\pi c x} \cdot \mathbf{1}\{x \in [c_-, c_+]\}. \quad (27)$$

with $c_{\pm} = 1 \pm \sqrt{c}$. In Fig. 2a we show the histogram of the singular values of \mathbf{W}/\sqrt{m} using Gaussian entries with zero mean and unit variance, when $m = 1024, n = 512$. We have also plot $f_{MP}(x)$. It follows that the largest singular value due to noise is approximately $1 + \sqrt{c}$. Thus, singular values



(a) Random matrix with i.i.d. entries. (b) Random matrix with Hankel structure.

Fig. 2: Normalized histograms of singular values (blue) and the quarter circle density (red).

associated to the signal that are below this threshold will not be differentiated from those of noise.

When the perturbation matrix has i.i.d. entries, experimental results have shown that threshold (26) leads to good performance, even when the SNR is negative. However, when considering a sum of exponentials, the perturbation matrix $\mathcal{H}_{\mathbf{w}}$ inherits the Hankel structure and its entries are not i.i.d. In this case, the empirical spectral distribution converges to a nonrandom symmetric probability measure which has no explicit expression [23]. Fig. 2b shows the histogram of the singular values of a matrix $\mathcal{H}_{\mathbf{w}}/\sqrt{m}$ with $m = 1024$, $n = 512$. In this case, there are singular values that fall outside the support of $f_{MP}(x)$, and choosing a threshold following (26) may lead to poor performance.

IV. RANDOM HANKEL MATRIX

Let λ_i and σ_i , $i = 1, \dots, n$, be the singular values of \mathcal{H}_x and \mathcal{H}_y respectively arranged in non-decreasing order. Following Weyl's Theorem we have that

$$|\sigma_i - \lambda_i| \leq \|\mathcal{H}_y - \mathcal{H}_x\|_2 = \|\mathcal{H}_{\mathbf{w}}\|_2 \quad (28)$$

Since $\text{rank}(\mathcal{H}_x) = r$, $\lambda_i = 0$ if $i > r$. Then

$$\sigma_n \leq \sigma_{n-1} \leq \dots \leq \sigma_{r+1} \leq \|\mathcal{H}_{\mathbf{w}}\|_2. \quad (29)$$

Lemma 2. Consider the complex vector $\mathbf{w} \in \mathbb{C}^{m+n-1}$. Let $\mathcal{H}_{\mathbf{w}}$, be the $m \times n$ Hankel matrix associated with \mathbf{w} . Then

$$\|\mathcal{H}_{\mathbf{w}}\|_2 \leq \max_{0 \leq k \leq m+n-2} |\mathbf{e}_{k+1}^T \mathbf{V} \mathbf{w}|, \quad (30)$$

where \mathbf{V} is the DFT matrix and \mathbf{e}_k is the k -th unitary vector.

Proof. See appendix A \square

Lemma 3. If $\mathbf{w} \sim \mathcal{CN}(\mathbf{0}, \eta^2 \mathbf{I}_{m+n-1})$, then

$$\mathbb{P}[\|\mathcal{H}_{\mathbf{w}}\|_2 \leq \tau] \geq \left[1 - e^{-\frac{\tau^2}{(m+n-1)\eta^2}} \right]^{m+n-1} \cdot \mathbf{1}\{\tau \geq 0\}. \quad (31)$$

Proof. See Appendix B \square

Theorem 3. Let $\mathcal{H}_{\mathbf{w}}$ be a $m \times n$ random Hankel matrix with generating vector $\mathbf{w} \sim \mathcal{CN}(\mathbf{0}, \eta^2 \mathbf{I}_{m+n-1})$. Then, for any $\beta \in [0, 1]$, we have that

$$\mathbb{P}[\|\mathcal{H}_{\mathbf{w}}\|_2 \leq \tau_1] \geq \beta.$$

where

$$\tau_1 = \sqrt{-(m+n-1)\eta^2 \log\left(1 - \beta^{\frac{1}{m+n-1}}\right)}. \quad (32)$$

Proof. The result follows from Lemma 3 by selecting β so that

$$\beta \leq \left[1 - e^{-\frac{\tau_1^2}{(m+n-1)\eta^2}} \right]^{m+n-1} \quad \square$$

When dealing with real random Hankel matrices, Lemma 3 is no longer valid, and we cannot follow the same path to obtain a bound on $\|\mathcal{H}_{\mathbf{w}}\|_2$. A possible solution is to perform Montecarlo simulations of the spectral norm of the Hankel matrix to obtain an empirical bound as in [24]. To avoid lengthy simulations, here we propose a workaround by using concentration inequalities.

Theorem 4. Let $\mathcal{H}_{\mathbf{w}}$ be a $m \times n$ random Hankel matrix with generating vector $\mathbf{w} \sim \mathcal{N}(\mathbf{0}, \eta^2 \mathbf{I}_{m+n-1})$. Then, for any $\beta \in [0, 1]$ we have that

$$\mathbb{P}[\|\mathcal{H}_{\mathbf{w}}\|_2 \leq \tau_2] \geq \beta.$$

where

$$\tau_2 = \sqrt{-2 \max\{m, n\} \eta^2 \log \frac{1-\beta}{(m+n)}} \quad (33)$$

Proof. Consider the following concentration inequality [13, chap. 4]

$$\mathbb{P}[\|\mathcal{H}_{\mathbf{w}}\|_2 \geq \tau] \leq (m+n) \exp\left[-\frac{\tau^2}{2\eta^2 \max\{m, n\}}\right]. \quad (34)$$

Then, the result follows by taking

$$\beta \leq 1 - (m+n) \exp\left[-\frac{\tau^2}{2\eta^2 \max\{m, n\}}\right] \quad \square$$

A bound similar to (33) was obtained in [12] for the case of real square Toeplitz matrices with gaussian elements. The bound we have just derived also works for rectangular matrices.

Bounds τ_1 and τ_2 establish hard thresholds that may be used as (26) to separate the signal space from the noise space. To compare these bounds, we have considered the case of real signals and square Hankel matrices, i.e., $m = n$. Since we are dealing with real matrices, we consider τ_2 as in (33). For square matrices, we compute the bound in (26) as

$$\tau_3 = \frac{4}{\sqrt{3}} \sqrt{n} \eta. \quad (35)$$

For each realization of the random vector $\mathbf{w} \sim \mathcal{N}(\mathbf{0}, \eta^2 \mathbf{I}_{2n-1})$, we compute the spectral norm of the associated square Hankel matrix. Fig. 3 shows the behavior of $\|\mathcal{H}_{\mathbf{w}}\|_2$ as the noise level η^2 increases. Each subplot corresponds to a different value of n . The shaded area represents the dispersion among the realizations of $\|\mathcal{H}_{\mathbf{w}}\|_2$ together with the bounds τ_2 and τ_3 .

As the matrix dimension increases, τ_3 approaches the mean value of $\|\mathcal{H}_{\mathbf{w}}\|_2$. As a consequence, when we estimate the order with τ_3 we take into account singular values associated with the noise subspace, as it was also observed in Fig. 2b. On the other hand, from Fig. 3 we see that τ_2 is a conservative

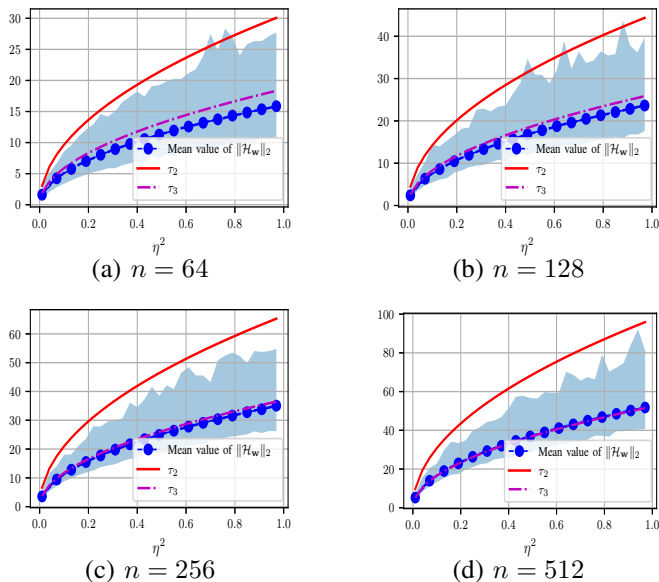


Fig. 3: Different realization of real and square $\|\mathcal{H}_w\|_2$ and bounds τ_2 , and τ_3 for different dimensions n with $\beta = 0.9$

bound, so some singular values corresponding to the signal subspace may fall under this threshold. To overcome this problem, in the next section we formulate a constrained optimization problem.

V. CONSTRAINED SELECTION RULE

We have observed that model order selection rules based on the singular value distribution of \mathcal{H}_y lose performance when strong signals are present because they do not consider the algebraic structure of the Hankel matrix. On the other hand, rules like ESTER or SAMOS underperform when the SNR is low because they are built on noise-free assumptions.

Here, we propose to combine both approaches in a single optimization problem to overcome both problems. In particular we impose a restriction on the singular values associated with the noise subspace. From inequality (29) we have

$$\sigma_{s+1} \leq \|\mathcal{H}_w\|_2 \leq \tau \quad (36)$$

with probability β . Notice that Theorems 3 and 4 give appropriate upper bounds for the singular values associated with the noise subspace. Based on these observations, we propose the following constrained optimization problem

$$\begin{aligned} \hat{r}_c &= \arg \min_{s \in \mathbb{N}} \mathcal{J}(s) \\ \text{s.t. } \sigma_{s+1} &< \tau, \text{ with probability } \beta. \end{aligned} \quad (37)$$

where $\mathcal{J}(s)$ can be either $J_{ESTER}(s)$ or $J_{SAMOS}(s)$ and τ is defined in Theorem 3 or 4 whether the noise is complex or real. The heuristic behind the constraint in (37) is as follows. Because this equation is an upper bound to the maximum singular value associated with the noise, all singular values bigger than τ correspond to those associated with the signal subspace. Let s^* be such that $\sigma_{s^*+1} < \tau < \sigma_{s^*}$. Then, the model order is at least s^* . Since (37) is a loose bound, the signal space may be larger, and some singular

values corresponding to the signal subspace may fall under the threshold. Nevertheless, the correct order minimizes (21) or (22) for $s \geq s^*$. In other words, we impose a maximum value to the singular values associated with the noise subspace. At the same time we penalize small orders selected with the ESTER rule. When taking τ_3 instead of τ_1 or τ_2 , we cannot claim that all singular values bigger than τ_3 correspond to the signal subspace.

VI. NUMERICAL EXPERIMENTS

We have compared the performance of the model order selection strategy proposed in (37) with those rules summarized in section III. We have performed Montecarlo simulations for different examples: three were taken from the literature, while the last one is introduced here.

A. Simulated models

Following the usual notation in the literature, we have considered the following model parametrization:

$$x_k = \sum_{i=1}^r a_i e^{\xi_i k} \quad (38)$$

where $\xi_i = 2\pi(\gamma_i + j\nu_i)$. Table I gives the values of the parameters for each example. Example 1 has two modes located close to each other, and the other two are farther apart. Example 2 is built by adding five more modes to Example 1. In particular, modes z_4, z_5 , and z_6 are clustered in a small region of the complex plane. The modes located in a small region of the complex plane may be confused by the model order selection strategy as a single mode. In Examples 3 and 4 explore further the issue. In both examples, we simulate one single large cluster, which may be obtained when a continuous-time system is digitized using a high sampling frequency. In Table I we summarize the parameter used in the numerical experimentation.

B. Analysis of results

For each example in Table I, we compare the following rules:

- \hat{r}_{thr} where τ is computed according to (26);
- \hat{r}_{ESTER} as in (21);
- \hat{r}_{SAMOS} as in (22);
- \hat{r}_c using the constrained selection rule as in (37) with $\mathcal{J}(s) = J_{\text{SAMOS}}(s)$ and $\tau = \tau_1$.

Our interest is to accomplish a qualitative comparison for different SNR regimes. Accordingly, we have varied the noise level, and for each SNR, we have considered $N = 5000$ independent realizations of (1). For the analysis, we have calculated the following performance metrics:

- Correct order estimation rate:

$$\text{COR} = \frac{\text{number of times } \hat{r} = r}{N}$$

- Histogram of order estimations.

The results are shown in Figures 4 and 5. In Fig. 5, we have performed an interpolation among values of consecutive

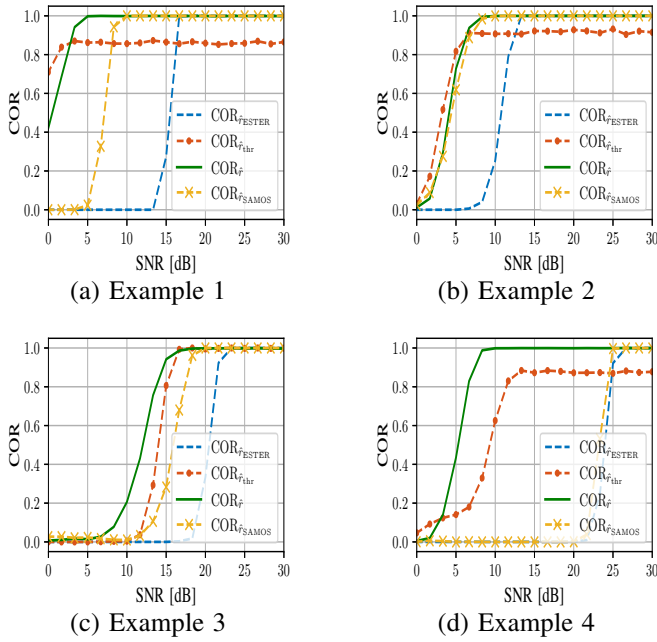


Fig. 4: Rate of correct order estimation (COR) as a function of the SNR.

histogram bins for visualization purposes only. By observing Fig. 4, we conclude that both ESTER and SAMOS rules have good performance when the SNR is high. However, they both fail to estimate the actual order when the SNR decreases. Notice that SAMOS performs better than ESTER in general. As stated in section III, the objective function in SAMOS is the average of the sine of all principle angles, while the objective function in ESTER is only the sine of the maximum

| | i | $\nu_i (\text{rad}^{-1})$ | $\gamma_i (\text{rad}^{-1})$ | $ a_i $ | $< a_i$ |
|----------------|-----|---------------------------|------------------------------|---------|---------|
| Example 1 [5] | 1 | -7.68 | -0.274 | 0.4 | -0.93 |
| | 2 | 39.68 | -0.150 | 1.2 | -1.55 |
| | 3 | 40.96 | 0.133 | 1.0 | -0.83 |
| | 4 | 99.84 | -0.221 | 0.9 | 0.07 |
| Example 2 [5] | 1 | -92.16 | 0.177 | 1.0 | 0.42 |
| | 2 | -7.68 | -0.274 | 1.5 | -0.95 |
| | 3 | 3.71 | -0.097 | 0.7 | 0.40 |
| | 4 | 11.90 | -0.116 | 0.6 | 0.02 |
| | 5 | 14.98 | -0.026 | 1.2 | -1.55 |
| | 6 | 19.20 | -0.327 | 0.4 | -0.93 |
| | 7 | 39.68 | -0.150 | 1.0 | -0.83 |
| | 8 | 40.96 | 0.133 | 0.9 | 0.009 |
| | 9 | 99.84 | -0.221 | 0.9 | 0.007 |
| Example 3 [17] | 1 | 0.2 | -0.01 | 1 | 0.00 |
| | 2 | 0.3 | -0.02 | 1.0 | 0.00 |
| | 3 | -0.2 | -0.1 | 2.0 | 0.00 |
| | 4 | 0.4 | -0.05 | 1.0 | 0.00 |
| | 5 | 0.35 | 0.03 | 1.0 | 0.00 |
| Example 4 | 1 | -0.22 | -0.01 | 0.97 | -1.78 |
| | 2 | -0.17 | -0.0037 | 1.58 | 2.89 |
| | 3 | -0.026 | -0.0058 | 1.14 | -2.46 |
| | 4 | 0.0037 | -0.012 | 0.96 | -1.15 |
| | 5 | 0.15 | -0.0089 | 1.12 | -0.32 |
| | 6 | 0.27 | -0.011 | 1.62 | 0.53 |

TABLE I: Parameters used in the numerical examples. The parametrization is as in (38).

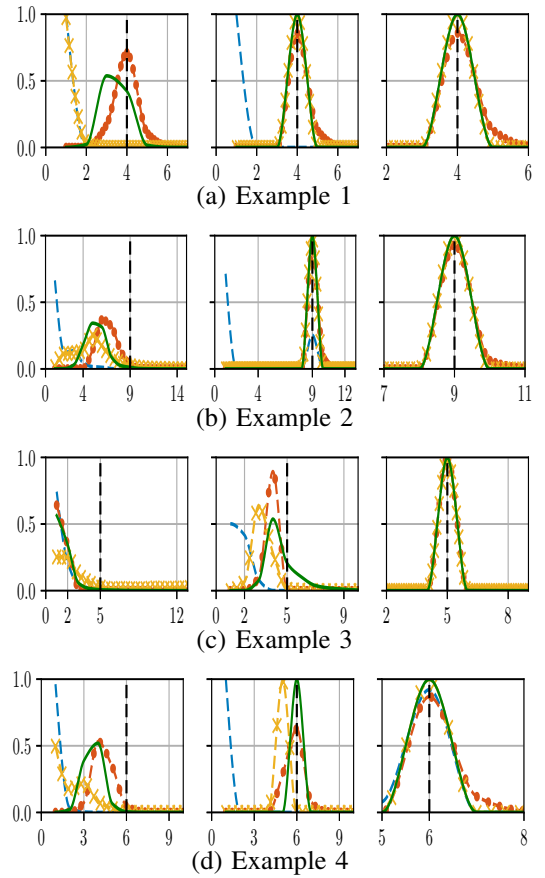


Fig. 5: Histograms of estimated order: \hat{r}_{ESTER} in (- -)blue, \hat{r}_c in solid green, \hat{r}_{thr} in (-•-) red, and \hat{r}_{SAMOS} in (-x-) yellow. Left columns correspond to SNR = 0dB, center columns to SNR = 10dB, rightmost columns to SNR = 25dB. The vertical dashed black lines denote the actual model order.

principal angle. On the other hand, \hat{r}_{thr} loses performance when the SNR increases. This last observation is explained by Fig. 5 where the histograms show that the optimal threshold rule tends to overestimate the model order when the SNR increases. Notice that the constraint selection rule can maintain the performance of the optimal selection rule at low SNR. Nonetheless, it also recovers the performance of the subspace-based selection rules when the SNR increases. Example 4 is of particular interest to test the behavior of the selection rules when several modes are clustered in a small region. While the constrained selection rule achieves good performance from 5dB on, ESTER and SAMOS require a SNR higher than 20dB for correct order estimation. Also, the optimal threshold cannot guarantee a correct order selection, even for large SNR.

VII. CONCLUSIONS

We have proposed a new model order selection rule for signals composed of sums of complex exponentials. This scheme benefits from the rotational invariance property of the Hankel matrix, which is beneficial when there is a good separation between the noise and the signal subspaces. But in the low SNR regime, the new scheme can retrieve the

actual model order by imposing a maximum bound on the noise contribution to the noisy Hankel matrix. This bound was proposed by analyzing the spectral norm of a random Hankel matrix. To test the performance of the proposed scheme, we have compared it with other selection rules from the literature. The results have shown a better performance of the constrained selection rule for most SNRs in all the examples that were considered.

APPENDIX

A. Proof of lemma 2

Let \mathbf{C}_w be the $(m+n-1) \times (m+n-1)$ circulant matrix associated with w . Then, using the definition of the circulant matrix, we express the $(m \times n)$ Hankel matrix \mathcal{H}_w as

$$\mathcal{H}_w = \begin{bmatrix} \mathbf{T}_m & \mathbf{0}_{m \times (n-1)} \end{bmatrix} \mathbf{C}_w \begin{bmatrix} \mathbf{0}_{(m-1) \times n} \\ \mathbf{I}_n \end{bmatrix},$$

where \mathbf{T}_m is an $m \times m$ exchange matrix (backward identity). Clearly,

$$\begin{aligned} \|\mathcal{H}_w\|_2 &\leq \left\| \begin{bmatrix} \mathbf{T}_m & \mathbf{0}_{m \times (n-1)} \end{bmatrix} \right\|_2 \|\mathbf{C}_w\|_2 \left\| \begin{bmatrix} \mathbf{0}_{(m-1) \times n} \\ \mathbf{I}_n \end{bmatrix} \right\|_2 \\ &\leq \|\mathbf{C}_w\|_2, \end{aligned}$$

where we have used the fact that

$$\left\| \begin{bmatrix} \mathbf{T}_m & \mathbf{0}_{m \times (n-1)} \end{bmatrix} \right\|_2 \leq 1, \quad \left\| \begin{bmatrix} \mathbf{0}_{(m-1) \times n} \\ \mathbf{I}_n \end{bmatrix} \right\|_2 \leq 1,$$

Since \mathbf{C}_w is a circulant matrix, its eigenvalues are $\mathbf{e}_{k+1}^T \mathbf{V} \mathbf{w}$. Then,

$$\|\mathcal{H}_w\|_2 \leq \|\mathbf{C}_w\|_2 = \max_k |\mathbf{e}_{k+1}^T \mathbf{V} \mathbf{w}|.$$

B. Proof of lemma 3

Using lemma 2, we know that $\|\mathcal{H}_w\| \leq \max_k |\mathbf{e}_{k+1}^T \mathbf{V} \mathbf{w}|$. Then, $\mathbb{P}[\|\mathcal{H}_w\| \leq \tau] \geq \mathbb{P}[\max_k |\mathbf{e}_{k+1}^T \mathbf{V} \mathbf{w}| \leq \tau]$.

Since w is a complex random vector with gaussian i.i.d. components and \mathbf{V} is DFT matrix without the normalizing factor $1/\sqrt{m+n-1}$, the vector $\mathbf{V} \mathbf{w}$ is an affine transformation which also has gaussian i.i.d. components. Moreover, $[\mathbf{V} \mathbf{w}]_i \sim \mathcal{CN}(0, (m+n-1)\eta^2)$ and $|[\mathbf{V} \mathbf{w}]_i|$ is Rayleigh distributed with parameter $\eta\sqrt{\frac{m+n-1}{2}}$. The distribution of the maximum is

$$\begin{aligned} \mathbb{P}(\max_k |\mathbf{e}_{k+1}^T \mathbf{V} \mathbf{w}| \leq \tau) &= \prod_{i=1}^{m+n-1} \mathbb{P}(|[\mathbf{V} \mathbf{w}]_i| \leq \tau) \\ &= \left[1 - e^{-\frac{\tau^2}{(m+n-1)\eta^2}} \right]^{m+n-1} \end{aligned}$$

for $\tau \geq 0$.

REFERENCES

- [1] T. K. Sarkar, Sheeyun Park, Jinhwan Koh, and S. M. Rao, "Application of the matrix pencil method for estimating the sem (singularity expansion method) poles of source-free transient responses from multiple look directions," *IEEE Transactions on Antennas and Propagation*, vol. 48, no. 4, pp. 612–618, 2000.
- [2] E. Gudmundson, P. Wirfält, A. Jakobsson, and M. Jansson, "An esprit-based parameter estimator for spectroscopic data," in *2012 IEEE Statistical Signal Processing Workshop (SSP)*, 2012, pp. 77–80.

- [3] J. Laroche, "The use of the matrix pencil method for the spectrum analysis of musical signals," *The Journal of the Acoustical Society of America*, vol. 94, no. 4, pp. 1958–1965, 1993. [Online]. Available: <https://doi.org/10.1121/1.407519>
- [4] P. Stoica and R. Moses, *Spectral Analysis of Signals*. Pearson Prentice Hall, 2005. [Online]. Available: <https://books.google.com.ar/books?id=h78ZAQAIAAJ>
- [5] F. Andersson, M. Carlsson, J. Tourneret, and H. Wendt, "A new frequency estimation method for equally and unequally spaced data," *IEEE Transactions on Signal Processing*, vol. 62, no. 21, pp. 5761–5774, 2014.
- [6] C. Grussler, A. Rantzer, and P. Giselsson, "Low-rank optimization with convex constraints," *IEEE Transactions on Automatic Control*, vol. 63, no. 11, pp. 4000–4007, 2018.
- [7] P. Stoica and Y. Selen, "Model-order selection: a review of information criterion rules," *IEEE Signal Processing Magazine*, vol. 21, no. 4, pp. 36–47, 2004.
- [8] A. Mariani, A. Giorgetti, and M. Chiani, "Model order selection based on information theoretic criteria: Design of the penalty," *IEEE Transactions on Signal Processing*, vol. 63, no. 11, pp. 2779–2789, 2015.
- [9] M. Gavish and D. L. Donoho, "The optimal hard threshold for singular values is $4/\sqrt{3}$," *IEEE Transactions on Information Theory*, vol. 60, no. 8, pp. 5040–5053, 2014.
- [10] —, "Optimal shrinkage of singular values," *IEEE Transactions on Information Theory*, vol. 63, no. 4, pp. 2137–2152, 2017.
- [11] S. Kritchman and B. Nadler, "Non-parametric detection of the number of signals: Hypothesis testing and random matrix theory," *IEEE Transactions on Signal Processing*, vol. 57, no. 10, pp. 3930–3941, 2009.
- [12] H. Qiao, "Estimating the number of sinusoids in additive sub-gaussian noise with finite measurements," *IEEE Signal Processing Letters*, vol. 27, pp. 1225–1229, 2020.
- [13] J. A. Tropp, "An introduction to matrix concentration inequalities," 2015.
- [14] J. M. Hokanson, "A data-driven mcmillan degree lower bound," *SIAM Journal on Scientific Computing*, vol. 42, no. 5, pp. A3447–A3461, 2020. [Online]. Available: <https://doi.org/10.1137/18M1194481>
- [15] R. Roy and T. Kailath, "Esprit-estimation of signal parameters via rotational invariance techniques," *IEEE Transactions on Acoustics, Speech, and Signal Processing*, vol. 37, no. 7, pp. 984–995, 1989.
- [16] R. Badeau, B. David, and G. Richard, "Selecting the modeling order for the esprit high resolution method: an alternative approach," in *2004 IEEE International Conference on Acoustics, Speech, and Signal Processing*, vol. 2, 2004, pp. ii–1025.
- [17] J. Papy, L. De Lathauwer, and S. Van Huffel, "A shift invariance-based order-selection technique for exponential data modelling," *IEEE Signal Processing Letters*, vol. 14, no. 7, pp. 473–476, 2007.
- [18] J. Razavilar, Y. Li, and K. Liu, "A structured low-rank matrix pencil for spectral estimation and system identification," *Signal Processing*, vol. 65, no. 3, pp. 363 – 372, 1998. [Online]. Available: <http://www.sciencedirect.com/science/article/pii/S0165168497002326>
- [19] R. Badeau, B. David, and G. Richard, "A new perturbation analysis for signal enumeration in rotational invariance techniques," *IEEE Transactions on Signal Processing*, vol. 54, no. 2, pp. 450–458, 2006.
- [20] G. Stewart and J. Sun, *Matrix Perturbation Theory*, ser. Computer Science and Scientific Computing. ACADEMIC PressINC, 1990.
- [21] R. A. Horn and C. R. Johnson, *Matrix Analysis, 2nd Ed.* Cambridge University Press, 2012.
- [22] N. J. Higham, "Matrix nearness problems and applications," in *Applications of Matrix Theory*, M. J. C. Gover and S. Barnett, Eds. Oxford University Press, 1989, pp. 1–27.
- [23] W. Bryc, A. Dembo, and T. Jiang, "Spectral measure of large random hankel, markov and toeplitz matrices," *The Annals of Probability*, vol. 34, no. 1, pp. 1–38, 2006. [Online]. Available: <http://www.jstor.org/stable/25449860>
- [24] R. J. Albert and C. G. Galarza, "Model order selection for sum of complex exponentials," in *2021 IEEE URUCON (IEEE URUCON 2021)*, virtual, Uruguay, Nov. 2021.